

# Multipath-Assisted On-Body Tag Localization

X. Liu (Author)

Faculty EEMCS

University of Twente

Enschede, Netherlands

x.liu-8@student.utwente.nl

Dr. P. T. de Boer (Committee Chair)

Dr. A. B. J. Kokkler (Committee Member)

Dr. Y. Miao (Daily Supervisor)

University of Twente

Enschede, Netherlands

Dr. I. Bilal (External Daily Supervisor)

Xsens

Enschede, Netherlands

**Abstract**—Active human localization with on-body radio device may suffer from performance degradation, due to self-body blockage during body movement, subject to the placing of tag on body and the position of anchor. In this paper, we present a strategy to use multipath and inertia motion data for Non Line-of-Sight (NLoS) body localization. We use an ultra-wideband (UWB) off-the-shelf Decawave kit for channel impulse response (CIR) acquisition, where a two-antenna anchor is fixed in space and a single-antenna tag is placed on a person’s chest. The multipath is extracted from the CIR at each snapshot by the non-super-resolution CLEAN algorithm, and the extracted multipaths are tracked during the body movement in space. Two types of body motions are considered: translational linear movement and rotational spin movement. Both Line-of-Sight (LoS) and NLoS scenarios are incorporated in numerical analysis. The results show that the multipaths’ track could well resemble the ground truth. On the other hand, inertia motion data such as angular velocity and orientation are measured during the body movement using the Xsens wearable Inertia Measurement Unit (IMU) sensor. Combining the multipath parameters and motion data, body’s positions under NLoS are able to be estimated.

**Index Terms**—Multipath, UWB, Human Localization, Body Motion.

## I. INTRODUCTION

Active human localization with on-body radio devices is to estimate a moving person’s position in space, based on the spatial information in the radio propagation channel between the on-body device and the other fixed device. Such application has shown great potential in many human-related areas, such as sports, medical and entertainment, where the position and movement information of persons are valuable [1], [2].

An active human localization radio system consists of two fundamental parts: anchors (fixed in position and orientation in space, reporting localization results to users) and on-body tags (attached on human’s body, communicating with anchor), as is shown in Fig. 1. The commonly embedded localization algorithm exploits direct LoS communication between an anchor and a tag, and estimates the position of the tag by applying time of arrival (ToA), phase difference of arrival (PDoA), or angle of arrival (AoA) techniques [3], [4]. Among all the radio localization technologies, UWB has proved itself to be an effective solution for localization with advantages of high delay resolution, low energy consumption, etc [3], [5]. The UWB pulse signals can easily penetrate through walls, clothing, which is an advantage when the localization environment is complex, e.g in indoor environment [5].

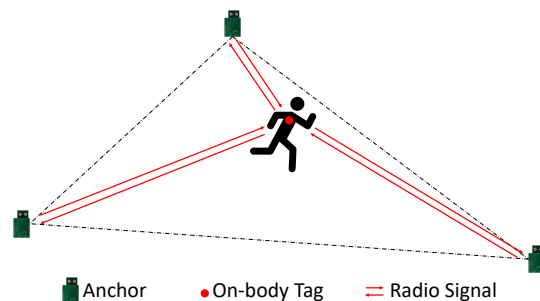


Fig. 1. Human Localization System

However, the signal will be significantly scattered by metallic and liquid materials [5]. This poses an issue specifically in human localization: considering the human subject’s mobility, the direct path between anchor and on-body tag may be blocked by the body itself (70% fluid) during movement, like what is shown in Fig. 2. In this case, the techniques using

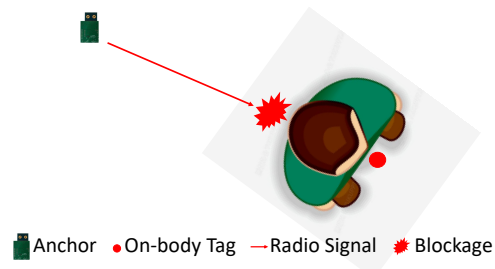


Fig. 2. Self-Body Blockage

direct path signals are not applicable any more, and result in low localization accuracy. One possible solution here is to make use of the multipath signals caused by the creeping waves around body or the reflection, diffraction, scattering from surrounding environment, and to associate this multipath information with human motion for localization, which yields as the purpose of this paper.

The rest of the paper is organized as follows. Section II gives an overview of previous research efforts and elaborates the motivation of the paper. Section III introduces the measurement campaign. An algorithm for on-body tag localization in NLoS scenarios are proposed in Section IV. Section V shows the

numerical analysis based on real-world measurement, where the performance of the algorithm is evaluated. Finally, the paper is concluded in Section VI.

## II. LITERATURE REVIEW AND MOTIVATION

As was introduced in previous section, active human localization suffers inaccuracy from self-body blockage caused by body movement. When the direct path is obstructed (OLoS scenario) or not available (NLoS scenario), researchers find solutions exploiting multipath other than the LOS path are needed. A simple method to tackle this problem is mentioned in [6], [7], the NLoS scenario is identified first, and under this scenario a particle filter, based on previous LoS localization results, is deployed to estimate the object's position under NLoS. Paper [8], [9] proposed techniques in mitigating NLoS localization bias, by extracting channel features as inputs for LOS/NLOS classification and ranging error regression reduction. Recently, the potential of using multipath for localization estimation has been investigated, as demonstrated in [10]–[15]. Multipath-assisted indoor navigation and tracking (MINT) are introduced in paper [10]–[12]. The basic principle of MINT is to associate multipaths extracted from channel measurement with the environment information, so that the multipath signals can be considered as direct path signal transmitted from virtual anchors (VAs) derived from the environment map, which is prior known to the user. In this case, the localization under NLoS showed improved robustness and accuracy compared with conventional measurement. Paper [13], [14] gave more advanced solutions in multipath assisted localization, namely simultaneous localization and mapping (SLAM), where the environment map and tag's position can be estimated simultaneously based on channel information without prior knowledge of the environment.

Inertial sensors are designed for motion measurement, which also yield potential in position estimation during objects' movements. Efforts have been made by combining IMU sensors and radio localization system to improve robustness, as are shown in [15]–[18]. In [16], [17], IMU data are fused with UWB localization output using extended Kalman filter (EKF), giving more precise positioning result compared to use either IMU or UWB alone. Paper [16] specifically addressed the NLoS and multipath effects in UWB ToA measurement, and by data fusion between IMU and UWB, the localization output showed increased position estimation accuracy under NLoS situation.

To summarize previous research efforts, localization under NLoS can be achieved using various techniques, among which multipath-assisted strategies exploiting the angular-delay information in radio channel demonstrated promising positioning results. However, in those projects the NLoS blockage was caused by environmental objects instead of self-body of the human beings. When it comes to on-body localization, the path shadowing characteristics caused by body blockage is more complicated, and the dynamic movement of body makes the changes in channel more unpredictable [19], [20]. To push forward the challenge, a multipath-assisted localization

strategy of a body-wear tag with special consideration of self-body blockage effect is needed.

This gives the motivation as well as the objective of this research. To our best knowledge, this is the first study on localizing on-body tag in NLOS scenario obstructed or blocked by self-body by using multipath channel parameters. In order to better understand the influence of self-body blockage on localization, channel measurement and analysis are needed where multipaths can be estimated for future NLoS localization estimation. Considering the dynamic change in channel is caused by human movement (e.g. body spin), it would be helpful if the motion data is measured at the same time which can be used for both channel investigation and localization estimation. The objective of exploiting multipath and IMU motion data for NLOS on-body tag localization is addressed in the following sections, starting with measurement of the channel and body movement, then the multipath-assisted localization algorithms, and finally validation of the results.

## III. CHANNEL ACQUISITION USING OFF-THE-SHELF RADIO SYSTEM

### A. Off-the-shelf Measurement System

1) *Radio System*: For channel acquisition in real-time, we used Decawave beta PDoA kit which can be deployed on body flexibly, including one anchor (DWM1002) and one tag (DWM1003), which is shown in Fig. 3. The products

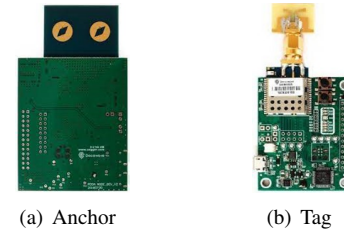


Fig. 3. UWB Measurement System

are embedded with a specific LOS-dependent localization algorithms, where Double-Side Two-Way Ranging (DS-TWR) are used for ranging detection and PDoA are used to determine the AoA [21], [22]. The DS-TWR derives the Time of Flight (ToF) and thereby the distance between anchor and tag by implementing three message exchange. The mechanism of DS-TWR is illustrated in Fig. 4(a). The three messages exchanged

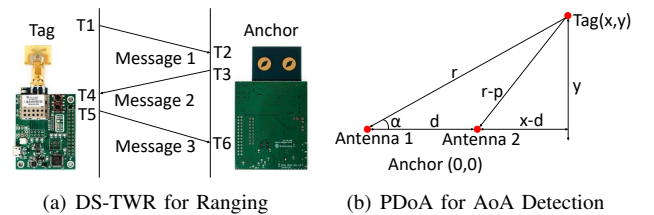


Fig. 4. Localization Mechanism embedded in the UWB Kit

between anchor and tag yield six timestamps ( $T1 - T6$ ), and the distance between anchor and tag can be derived from the

TABLE I  
RADIO SYSTEM PARAMETERS

Parameter	Value
Center Frequency	3.5 GHz
Bandwidth	500 MHz
Antenna	DWM1003 (CP-Wings antenna) DWM1002 (Mona-Lisa antenna)

timestamps by averaging the time interval of two round trips ( $T_4 - T_1$  and  $T_6 - T_3$ ). For embedded AoA detection, the anchor uses two antennas to receive a message to determine the phase difference between the two, like what is shown in Fig. 4(b).  $r$  is the ranging result measured from DS-TWR, and  $d$  is the known distance between two antennas. With information of phase difference of the arrival signals at the two antennas,  $p$  can be calculated and the coordinate of tag with regard to anchor can be further derived.

With a purpose for product development and diagnostics, the kit also records CIR data during localization measurement so that users can visualize the radio channel. The CIRs were measured at a temporal sampling rate of 1 Hz, at each snapshot the CIRs contain 1016 complex data points, with a delay resolution of 1 ns. Table I demonstrates the measurement specifications. In addition, 3-D radiation pattern plots of the antennas on both anchor and tag are shown in Fig. 5.

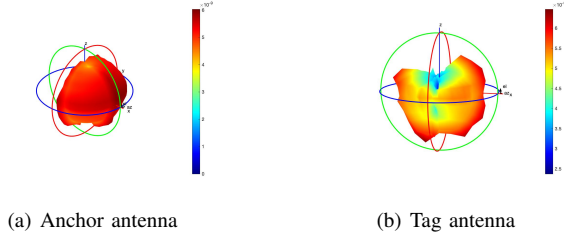


Fig. 5. Radiation Pattern of Decawave UWB Kit. In this paper, we assume the antennas are isotropic in the orientation direction

2) *Inertia sensor*: With the goal of tracking the motions of human or vehicles, IMUs are located in target subjects during the movement, measuring the motion data simultaneously. Therefore here we attached Xsens Dot (shown in Fig. 6(a)), an wearable IMU sensor, to the tag so that motion data of the body was recorded at the same time (shown in Fig. 6(b)).

The motion data that is available from Xsens Dot includes angular velocity, orientation, and free acceleration in three dimensions [23]. With  $2.0^\circ$  RMS orientation accuracy, the sensor is able to specify the heading of body during movement. Such information will be used in localization algorithm in Section IV.

### B. Measurement Campaign

During measurement, the anchor is fixed in certain position by a tripod, and the tag is located on human's body, in a manner of held by a single hand at the middle of the chest, as

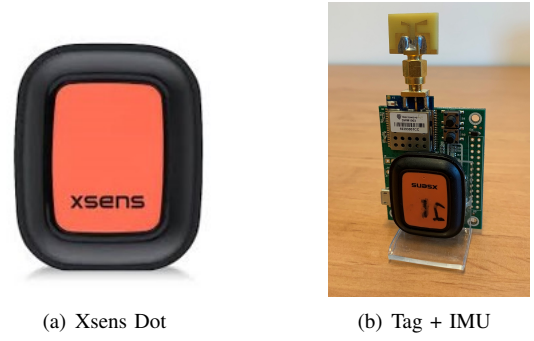


Fig. 6. Motion Measurement System

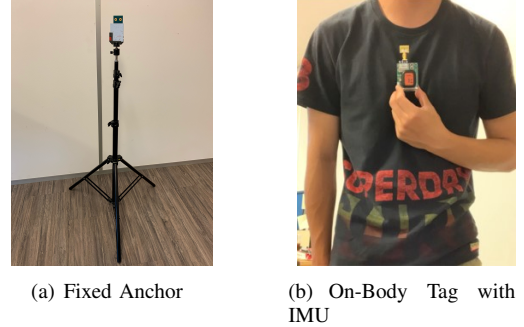


Fig. 7. Measurement Setup: Anchor and Tag

are shown in Fig. 7. While a person have such tag positioned on the body, who was doing two kinds of motions, namely linear walking and spin, illustrated in Fig. 8 & below:

- 1) The person always faced to the same direction and moved along a straight line with the speed of about 0.1 m/s; the anchor was fixed at one end of the person's trajectory, we recorded two trajectories: 1) the person's chest faced to the anchor (LoS) and 2) the person's back faced to the anchor (NLoS);
- 2) The person stood at certain position, starting from facing directly to the anchor and then slowly spin the body for 360 degrees in a speed of about 6 degree/s, experiencing transitions from LoS, to obstructed-LoS (OLOs), to NLoS, and then back to OLoS and LoS eventually.

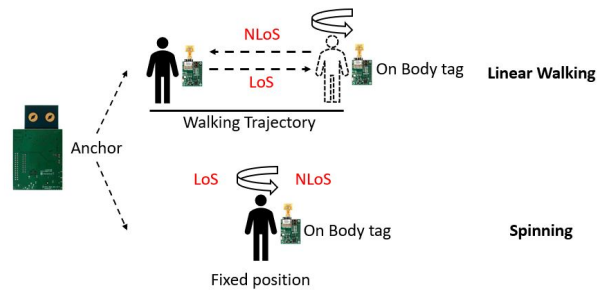


Fig. 8. Motion Pattern

These two kinds of motion are considered essential for the following reasons. First, these two kinds of motions reflect

the typical behavior of normal pedestrian. Second, channel changes during these two motion are critical to for LOS/NLOS localization. The body obstruction then blockage may start when human gradually spin the body, in this case we can expect significant attenuation on direct path signal and the rising of the NLoS multipath from the channel measurement. For both motion patterns, it is important to find out how the multipaths change in accordance with the change of positions, which is the key in designing localization strategy using multipaths in case of NLoS.

The measurement was designed to be carried out under three scenarios: free space, one wall and two walls environment. These three scenarios are shown in Fig. 9. During measurement, the tag is hand-held at the middle of the human’s chest. The reason to hold the tag by hand is trying to reduce the unpredictable influence on measurement caused by cloth or accident body collision on the tag’s antenna. Compared to the way where the tag is attached to the body using strap, the possibility of frictions between antenna and body is reduced to the minimum.

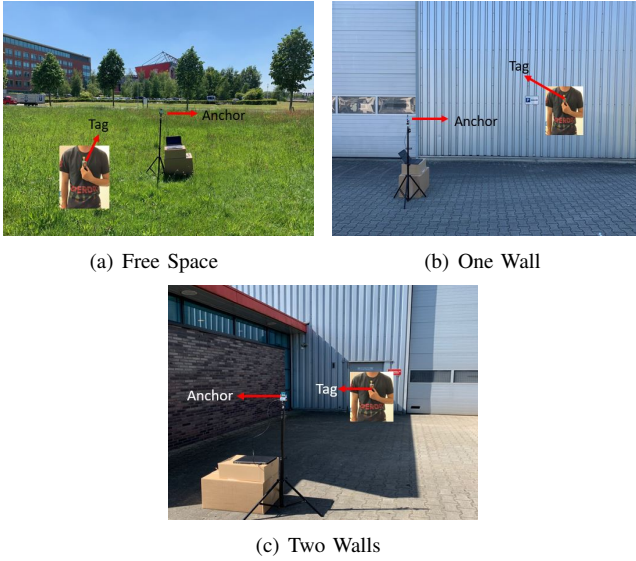


Fig. 9. Measurement Scenarios

The major consideration behind the scenario design is the complexity of environment, which directly determines the multipaths situation. Walls in scenario (b) and (c) are expected as strong sources of multipaths. By increasing the number of major scatterers, more multipaths will emerge and can be used for later localization estimation.

#### IV. METHODOLOGY

In this section, the methodology used for multipath-assist on-body tag localization are introduced. First, the flow chart of the overall proposed framework is shown in Fig. 10. The framework starts with knowledge of the environment map, and we assume that the human is either walking linearly or spin with position unchanged, and the motion process starts from LoS. Each component in the flowchart will be introduced within this section.

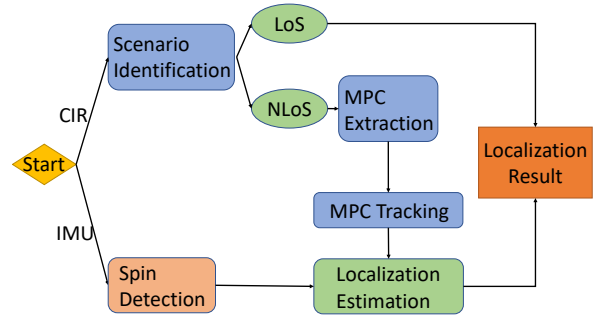


Fig. 10. Overview Algorithms

#### A. Scenario Identification

The first step of the overall algorithm is to distinguish between LoS and NLoS. The motivation behind this step is to separate the localization measurement results from the embedded algorithm in the UWB kit, so that the LoS measurement can be kept as trusted position results, while the NLoS results will be discarded, and localization estimation will be made under this scenario. This scenario identification algorithm make uses of the CIR measured at each temporal sample, and this multipath channel is modelled in the delay domain as follows:

$$h(t, \tau) = \sum_{l=1}^{L_t} \alpha_l(t) \delta(\tau - \tau_l(t)) \quad (1)$$

where  $l$  is the peak index,  $L_t$  is the total number of peaks in the impulse response,  $t$  indicates the temporal sample,  $\alpha_l(t)$  is the complex gain of the  $l$ -th peak, and  $\tau_l(t)$  is the corresponding delay bin.

The scenario identification uses CIRs as data input, and determine the probability of LoS or NLoS based on different channel characteristics under these two scenarios. These different characteristic are illustrated as follows. First characteristic is the delay difference between first peak and highest peak in the CIR. Consider a LoS scenario where the direct path signal is well received without any scattering or blockage, the first peak is highly likely to be the strongest peak among all the impulse responses, in this case if we calculate the delay difference between the highest peak and the first peak, the difference would be rather small, as is shown in Fig. 11(a). However, in OLoS and NLoS case the direct path is usually significantly attenuated or fully blocked. At this time the highest peak in this CIR may be one of the multipaths, and will be certain delay away from the first peak, like Fig. 11(b). This gives us one inspiration to distinguish LoS / NLoS: if the delay difference between the first peak and highest peak in CIR can be derived, we can use such information to estimate the probability of LoS or NLoS.

The second channel characteristic that we use for scenario identification is delay spread, and the reason behind this is also straight forward: if there is LoS, the most of the CIR power will gather around the delay bins of the direct path

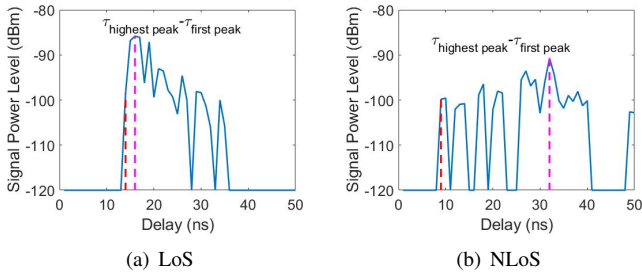


Fig. 11. Characteristic 1

signal, while under NLoS the power will spread to a larger delay range than LoS, as are shown in Fig. 12. To show the delay spread of the major part of the total CIR power and to try to neglect the noise energy, delay spread of 70% of the total CIR power is given.

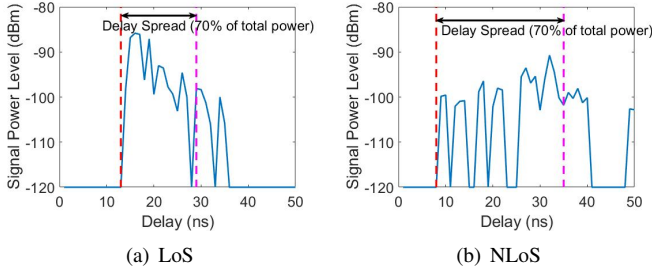


Fig. 12. Characteristic 2

With these two characteristics in mind, the scenario identification strategy is designed. By computing the delay bin difference of the first peak (FP) and the highest peak (HP), and the delay spread of 70% of the total CIR power:

$$c1 = \tau_{HP} - \tau_{FP} \quad (2)$$

$$c2 = \tau_{70\%power} = \arg(\sum_{l=1} |h(\tau_l)|_{0.7P_{total}}) \quad (3)$$

Determine the LoS / NLoS range for the two values based on observation of the measurement, and define an identification function to decide the probability of NLoS, with input the calculated value of  $c1$ ,  $c2$ , and the output  $P_{NLoS}$  normalized between  $[0, 1]$ , indicating the chance that the propagation scenario being NLoS:

```

if  $c \leq c_{LoS}$  then
   $P_{NLoS} \leftarrow 0$ 
else
  if  $c \geq c_{LoS}$  &  $c \leq c_{NLoS}$  then
     $P_{NLoS} \leftarrow \frac{\exp(\lambda * (c - c_{LoS})) - 1}{\exp(\lambda * c_{NLoS}) - 1}$ 
  else
     $P_{NLoS} \leftarrow 1$ 
  end if
end if

```

An example of this function is given in Fig. 13.

$c_{LoS}$ ,  $c_{NLoS}$  for  $c1$   $c2$ , as well as the rate parameter  $\lambda$  for two characteristics are empirically determined by measurement and testing results of over 9000 sampling points. Each of these

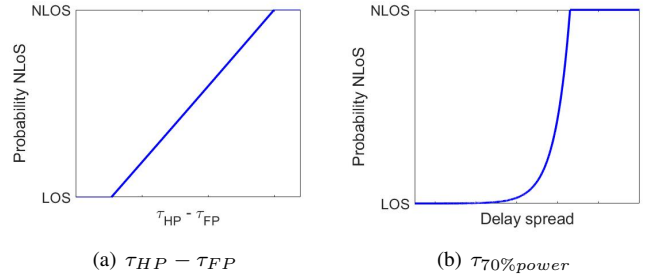


Fig. 13. Scenario identification functions, with x-axis the value of  $c1$  and  $c2$ , and y-axis the cumulative probability of NLoS

two function gives a NLoS probability, and the final result is averaged over the two probabilities. If the final result has a value over 0.5, the scenario at this time will be identified as NLoS, in this case, further process is needed for localization estimation; otherwise, the scenario will be considered as LoS, and the measured localization result will be trusted.

With over 9000 temporal samples measured and tested under the three above mentioned scenario, the scenario identification algorithm showed robust performance with an identification accuracy of 95%, validated with the help of inertial measurement.

### B. MPC Extraction

After the LoS and NLoS scenarios are identified, the next step is to make analysis of the measured channel information, and to extract the multipaths for later uses. In this paper, CLEAN algorithm is used to extract the high peaks, which are the MPC candidates, from the CIR. The CLEAN algorithm is first introduced in [24], which iteratively operated on the radio sky map to distinguish the real structure from the dirty map. The algorithm is widely used in channel processing, like the work in [25], [26]. Despite algorithms like MUSIC and SAGE [27], [28] with super-resolution multipaths extraction, this non-super-resolution CLEAN algorithm works well with the UWB time domain measurement and is sufficient because of the high delay resolution.

The basic principle of this CLEAN algorithm is to search for the strongest peaks in the CIR, save this as extracted multipath, subtract this multipath from frequency domain, then transfer to time domain and search for the next multipath. Specifically, first we search for the highest peak from the measured CIR:

$$\tau_i = \arg \max_{\tau} \sum_{l=1}^L h(\tau_l) \quad (4)$$

The  $i$ -th multipath is then saved with the parameter  $(\tau_i, \alpha_i)$ , while  $\alpha_i$  is the complex gain at delay bin  $\tau_i$ . Then, we subtract this multipath in the frequency domain. The channel transfer function with frequency  $f_k$  can be derived by a Fourier transform of the CIR [29]:

$$H_t(f_k) = DFT[h_t(\tau_l)] = \sum_{l=1}^L [\alpha_l \exp(-j2\pi f_k \tau_l)] \quad (5)$$

Delete MPC  $i$  from the transfer function, and the portion of this peak over all the sampling point on frequency domain will be removed:

$$\widehat{H}_t(f_k) = H_t(f_k) - \alpha_i \exp(-j2\pi f_k \tau_i) \quad (6)$$

Then transform  $\widehat{H}_t(f_k)$  back into time domain to search for the next MPC:

$$\widehat{h}_t(\tau_l) = IDFT[\widehat{H}_t(f_k)] = \frac{1}{K} \sum_{k=1}^K \widehat{H}_t(f_k) \exp(j2\pi f_k \tau_l) \quad (7)$$

Where  $K$  is the number of sampling points in frequency domain. After the extraction of one peak is done, search for the next multipath from the current impulse response. In this research, only the major MPCs will be investigated, therefore the algorithm will keep extracting the multipaths until the extracted MPCs contain more than certain percentage of the total CIR energy, depending on how much multipaths we expect from the extraction. By extracting such energy proportion of the total power, the major scattered signals can be well obtained, as will be shown in later sections.

By the end of the MPC extraction algorithm, a set of  $N_t$  multipaths are derived from the CIR at the current temporal sample  $t$  at both channels, and the multipaths are saved in a set by their multipath parameters (where  $i \in 1 \dots N_t$ ):

$$\text{Peaks}(i, t) = \begin{pmatrix} \tau_p(i, t) \\ \alpha_p(i, t) \end{pmatrix} \quad (8)$$

### C. MPC Tracking

The MPC extraction provides us with extracted multipaths at each temporal sample. The next step is to track the multipath over time steps, so that the dynamic change of multipaths over spatial-temporal transitions can be observed, which can be further associated with body movement and used for localization estimation. MPC tracking is widely used in radio-sensing, especially the ones with multipaths assistance, such as [30]–[35]. [31]–[33], [35] tackled the multipaths tracking as probabilistic problems, using particle filters [33], [35] or EKFs [31], [32].

Paper [34] proposed a computational-efficient algorithm to track wideband multipaths signals. The basic principle is to search the MPC at current time step, based on the MPC parameters at the previous time steps, with consideration of the changing rate. Fig. 14 illustrate the scheme of the tracking algorithm. The vertical axis indicates the evolve of time, while horizontal axis represents the MPCs parameters (delay and signal amplitude). The black dots from  $t-4$  to  $t-1$ , belong to one tracked multipath. The goal at this time is to search among all extracted multipaths (shown as white dots) in temporal sample  $t$ , and identify the previously tracked multipath at this time. In order to do this, the algorithm take the multipath change ( $\Delta\tau$  and  $\Delta\alpha$ ) into consideration, define a searching window at temporal sample  $t$ , and find the suitable MPC candidate.

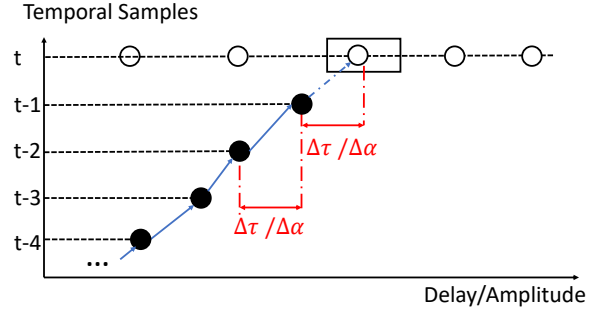


Fig. 14. MPC Tracking

The algorithm starts at the multipath with the highest power extracted from the first time step, Considering it as the first multipath ( $j = 1$ ) tracked at the beginning ( $t = 1$ ):

$$\text{MPC}(j, t)|_{j=1, t=1} = \begin{pmatrix} \tau_m(1, 1) \\ \alpha_m(1, 1) \end{pmatrix} = \max_{\alpha} \text{Peaks}(t = 1) \quad (9)$$

Starting from this multipath, the algorithm tracks its trajectory in the next temporal instances. In order to do this, it searches for neighboring peaks of the current multipath at next temporal step. In order to find the position of MPC(1, 1) at  $t = 2$ :

$$\text{MPC}(1, t)|_{t=2} = \arg \min_{\text{Peaks}} d[\text{MPC}(j, t), \text{Peaks}(t + 1)] \quad (10)$$

In (10),  $d[.,.]$  is defined as:

$$d[\text{MPC}(j, t), \text{Peaks}(t + 1)] = \begin{pmatrix} \tau_m(j, t) - \{\tau_p(i, t + 1)\}_{i=1}^{N(t+1)} \\ \alpha_m(j, t) - \{\alpha_p(i, t + 1)\}_{i=1}^{N(t+1)} \end{pmatrix} \quad (11)$$

In order to prevent the current multipath converging with other multipaths, a searching window is defined to restrict the MPC tracking:

$$X(j, t) = \begin{cases} 1 & \text{if } d(\text{MPC}(j, t - 1), \text{Peaks}(t)) \leq \delta \\ 0 & \text{Otherwise} \end{cases} \quad (12)$$

$X(j, t)$  here is defined as MPC status parameter, indicating whether the  $j$ -th multipath can be tracked at time step  $t$ . If within a searching window  $(-\delta, \delta)$  no multipath can be found,  $X(j, t)$  will be set to 0, meaning the current multipath disappears at this time. Otherwise,  $X(j, t)$  will be set to 1, meaning the multipath is still alive, and choose the closest peak to the MPC( $j, t - 1$ ) as the position of this multipath at  $t$ , like what is done in (10).

Considering the object is moving, starting from  $t = 3$  the MPC tracking updates the change of multipath trajectory, namely  $\delta_{\text{MPC}}(j, t)$ :

$$\Delta_{\text{MPC}}(j, t) = d[\text{MPC}(j, t - 1), \text{MPC}(j, t)] \quad (13)$$

and the searching rules for  $t \geq 3$  is described in (14):

$$\text{MPC}(j, t)|_{t \geq 3} = \arg \min_{\text{Peaks}} d[\text{MPC}(j, t - 1) + \Delta_{\text{MPC}}(j, t - 1), \text{Peaks}(t)] \quad (14)$$

Note that the algorithm can not identify the sudden emerging multipaths, which sets an limitation on the robustness of the algorithm. To track such multipaths, we need manually define the start of these multipaths, and run the algorithms to track them along time samples.

With the above mentioned algorithm, multipaths can be well tracked from their births till they disappear. After MPC tracking, we can obtain the trajectories of one or more multipaths evolve over time, which will be used later in position estimation.

#### D. Spin Move Detection Using IMU

So far we have already got sufficient multipaths information from channel measurement and analysis. On the other hand, we have the motion measurement from Xsens Dot. The next step is to parse the measured data, synchronize it with channel measurement, and associate these two for localization.

As is mentioned in Section III B, there are two kinds of motion investigated in this research: linear walking and spin. Since the NLoS is caused by body blockage and the blockage is usually caused by changes of the human's heading, spin detection becomes an critical part in this research. With the measurement from IMU, it is possible for us to detect when the spin happens, how long does the body spin and how many degrees does the body spin.

To detect body spin, two types of data will be used from IMU: orientation and angular velocity. When a spin starts, a sudden increase on angular velocity will be observed, and the velocity value will remain relatively high till then end of the spin. When the body spins, we can also notice that the orientation measurement will varies within the defined range from  $-180^\circ$  to  $180^\circ$ . With information about when the spin starts and ends, the orientation difference can be derived. Based on these observation, we use angular velocity as trigger for determine the start and end of spin, and record the orientation change during the identified spin process. Before introducing the detection algorithm, first an example of angular velocity and orientation measurement is shown in Fig. 15. The measurement showed that during spin, the angular velocity was fluctuating around a higher level than non-spin time. To eliminate the effect of data fluctuation, the algorithm calculate the sum of three consecutive angular velocity value, and decide at this time the body is spinning if the sum value exceed a threshold.

$$Spin(t) = \begin{cases} 1 & \text{if } \sum_t^{t+2} V_{angle} \geq \mu \\ 0 & \text{Otherwise} \end{cases} \quad (15)$$

$Spin(t)$  is the state vector for body spin, with a value of 1 indicating the body is spinning at temporal sample  $t$ .  $\mu$  is the threshold, which is derived from measurement observation.  $Spin(t)$  contains information about the start and end of different body spins, and the spin degrees of the  $j$ -th spin can be derived accordingly from the orientation measurement following the Eqn. 16, where  $Orientation(t)$  is the orientation measurement from IMU.

$$\Delta\phi(j) = Orientation(t) \Big|_{t_{spin(j)start}}^{t_{spin(j)end}} \quad (16)$$

The orientation of the tag should be calibrated with the anchor's position. In this research, we make the initial orientation  $Orientation(t=0) = 0$ .

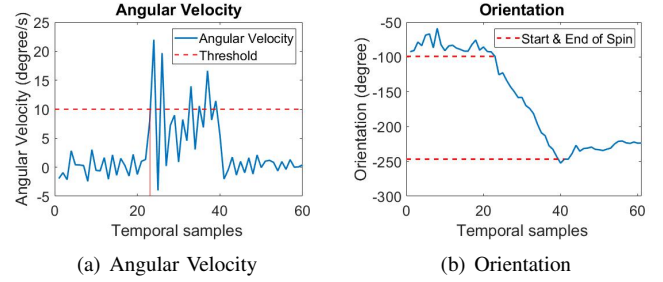


Fig. 15. Scenario Identification Functions

#### E. Localization

With the above derived results, we proceed to the final step of the whole algorithm: localization under NLoS. So far, we have already obtained the extracted and tracked multipaths, body motion data with spin motion specifically recognized, and the multipaths trajectories and body motion data are temporally synchronized.

The localization strategy is based on the Virtual Anchor (VA) concept [10]–[12]. In this research, we assume that the multipaths that could be tracked are caused by reflection from major scatterer, e.g. big wall. If the ground truth is known at the first place, i.e. the positions of major scatterers with regard to the fixed anchor are available, we could mirror this physical anchor at the scatterers' surfaces, so that we have VAs corresponding to these reflections. In this case, the multipaths can be associated with the VAs, as the direct paths from the VAs to the tag, as illustrated in Fig. 16:

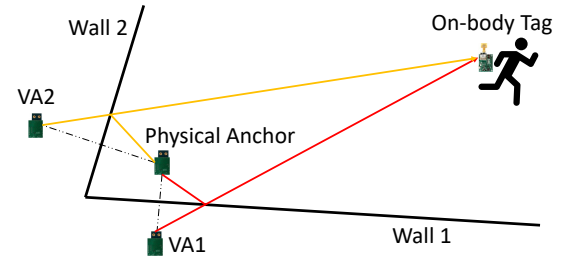


Fig. 16. Illustration of the 2-D floorplan and the VA concept. The multipaths from the two wall (yellow and red line) are associated with the VAs from the two walls, which are then considered as direct paths from VAs to tag

Theoretically, virtual anchor can be used alone for multipath-assisted localization algorithms, if the multipaths are accurately tracked. However, according to the performance of our tracking algorithm, we noticed that the multipath trajectory is shifted on delay bin compared with the ground truth, which will be further discussed in Section V.A.

With this delay shift of tracked multipaths, we cannot simply depend on VAs to estimate the tag's position since the

inaccurate propagation delay of these multipaths will lead to high error on ranging estimation. This means we will not use the absolute delay of each multipath for ranging estimation at each temporal sample. Instead, we make use of the change of multipath between temporal samples, to calculate the position change of the moving tag, with the help of body motion data and environmental information. Hereby, we present our localization strategy under NLoS as following.

The human, wearing the tag, either linearly walk or spin in this research, as is mentioned before. We assume the human starts with LoS, and randomly performing one of the two motion patterns. The starting orientation with regard to the anchor  $\phi_0$  is also known. First, we look at the spin detection. In case a body spin happens, we check:

- 1) Whether there is changing from LoS to NLoS, according to scenario identification;
- 2) How much degree does the body spin

If after the spin, the LoS does not change, then we keep outputting the localization measurement. Otherwise, it means self body blockage happens due to body movement. At this time, localization measurement will not be trusted. To estimate the position of tag, we first retrieve the following information. Assuming the  $j$ -th body spin starts at temporal sample  $t_0$ , spinning during a period of  $\Delta t_{spin(j)}$ :

- 1) The position when the body spins from LoS to NLoS  $P(t_0)$ ;
- 2) The orientation when the body stops spin  $\phi(t_0 + \Delta t_{spin(j)}) = \phi(t_0) + \Delta\phi(j)$
- 3) The tracked multipaths during the spin process

As we known, the position change after spin, under NLoS, always resulted by linear walking, where the heading of human remains unchanged. In this case, we can imagine a straight walking trajectory of this people, and the position results are distributed points on this line, as is shown in Fig. 17. The changing of these position points will be further associated with body movement.

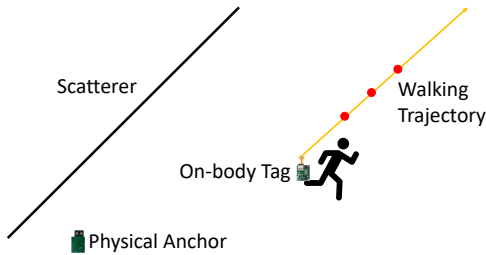


Fig. 17. With fixed orientation after spin, the human moves towards the same position, indicating that the future localization results, shown by the red dots, can be derived on the walking trajectory

With this NLoS walking trajectory determined, the next step is to localize the body along the trajectory at each temporal sample, till the next body spin happens. In this step, the tracked multipaths information is used. Specifically, we choose one multipath that we could track after the spin, here for example

the  $MPC(j, t_0 + \Delta t_{spin(j)})$ , which is tracked we calculated the multipath delay change between the consecutive temporal samples:

$$\Delta\tau_m(j) = \tau_m(j, t_0 + \Delta t_{spin(j)} + 1) - \tau_m(j, t_0 + \Delta t_{spin(j)}) \quad (17)$$

and then convert the delay difference into path length difference (1 nanosecond delay bin is equivalent to 0.3 meters of path difference):

$$\Delta P_{MPC(j)} \Big|_{t_0 + \Delta t_{spin(j)}}^{t_0 + \Delta t_{spin(j)} + 1} = \Delta\tau_m(j) \cdot 0.3 \quad (18)$$

Then we look at the position when the spin ends, which we consider unchanged compared to the position when the spin starts. Suppose the position of the human when the spin starts is  $P(t_0) = (x(t_0), y(t_0))$ :

$$P(t_0 + \Delta t_{spin(j)}) = P(t_0) \quad (19)$$

From the ground truth, we have the position of  $VA_j$  that originate  $MPC(j, t_0 + \Delta t_{spin(j)})$ , which is denoted as  $P_{VA_j} = (x_{VA_j}, y_{VA_j})$ . Then, the distance between  $VA_j$  and the on-body tag during spin can be calculated from:

$$d(t_0) = \sqrt{(x(t_0) - x_{VA_j})^2 + (y(t_0) - y_{VA_j})^2} \quad (20)$$

Eqn 20 tackles the issue of delay shift of the multipaths trajectory, since the distance between VA and tag is calculated using ground truth and accurate localization measurement. At time step  $t_0 + \Delta t_{spin(j)}$ , the spin ends and the human start to walk. Till the next temporal sample  $t_0 + \Delta t_{spin(j)} + 1$ , we have the multipath change  $\Delta P_{MPC(j)} \Big|_{t_0 + \Delta t_{spin(j)}}^{t_0 + \Delta t_{spin(j)} + 1}$ . Add the multipath change to  $d(t_0)$ , we have

$$d'(t_0 + \Delta t_{spin(j)}) = d(t_0) + \Delta P_{MPC(j)} \Big|_{t_0 + \Delta t_{spin(j)}}^{t_0 + \Delta t_{spin(j)} + 1} \quad (21)$$

To make the steps more intuitive, Fig. 18 illustrate the localization with parameters. According to the Fig. 18, we only need  $\Delta P$  to determine the position at next time step. With the orientation measurement as well as the ground truth, the angle between  $MPC_j$  at  $t_0 + \Delta t_{spin(j)}$  and the walking trajectory  $\alpha(t_0 + \Delta t_{spin(j)})$  can be derived. With  $\alpha(t_0 + \Delta t_{spin(j)})$ ,  $d(t_0 + \Delta t_{spin(j)} + 1)$  and  $d'(t_0 + \Delta t_{spin(j)})$ , the problem to derive  $\Delta P$  simply become a "side-side-angle" triangle solving problem. With off-the-shelf triangle solving algorithm,  $\Delta P$  can be derived, and the localization result at temporal sample  $t_0 + \Delta t_{spin(j)} + 1$  is denoted as:

$$P(t_0 + \Delta t_{spin(j)} + 1) = P(t_0 + \Delta t_{spin(j)}) + \Delta P(\cos \beta, \sin \beta) \quad (22)$$

Repeat the previous steps, update  $d$ ,  $d'$ ,  $\alpha$  and  $\beta$  for every time steps under NLoS until the next spin, or there is change from NLoS to LoS.

## V. NUMERICAL ANALYSIS

### A. Multipath Extraction and Tracking

In this section, the channel measurement and analysis are presented. Specifically, we measured the spin and linear walking under the three scenarios introduced in Section III. After

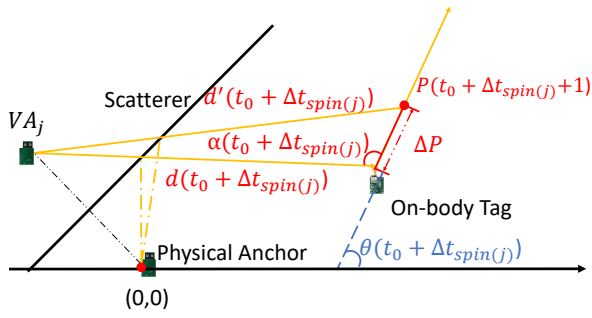


Fig. 18. localization

measurement, channel analysis are performed on the results, where multipath extraction and tracking are implemented. First, the linear walking and spin in free space scenario: Fig.

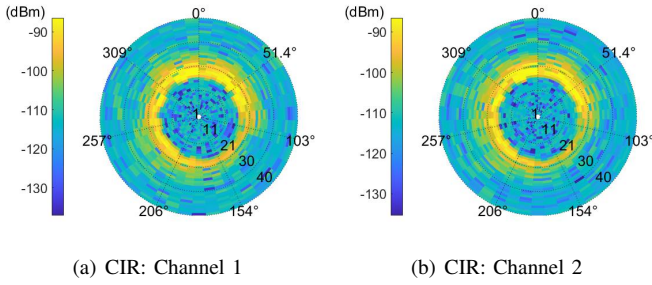


Fig. 19. Channel measurement for a 360 degree spin process

19 shows the raw channel measurement for a complete spin motion in a polarplot, with the radius indicating delay bin and color indicates the path power. The spin motion started when the person faced to the anchor at 0 degree, and after 360 degree slow spin the person faced to the anchor again. With CIR obtained, we extracted the major peaks from it, and the results are displayed in Fig. 20.

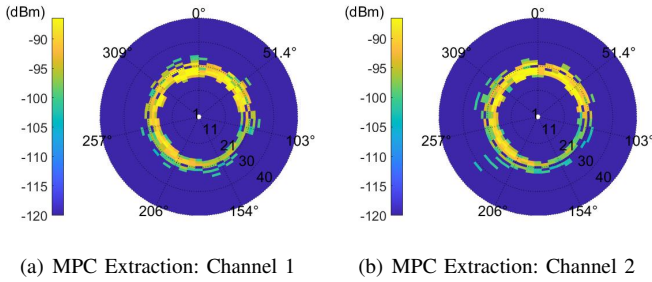


Fig. 20. Multipath extraction from previous channel measurement

The major path signals, clustering around delay bin  $\tau = 23$ , are extracted from the noisy impulse responses. Based on the extraction results, the multipath (in this free-space case, the direct path) is tracked over time, shown in Fig. 21.

From the extraction and tracking result, we can observe the following characteristics:

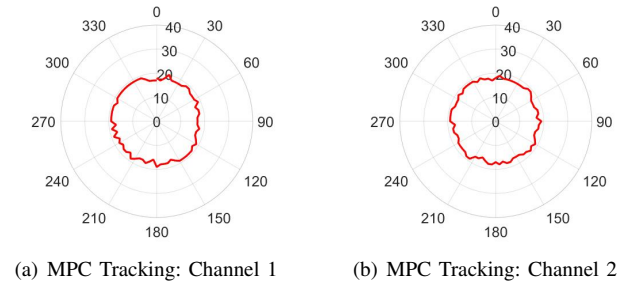


Fig. 21. Multipath tracking over temporal samples

- 1) Despite the direct path is attenuated when the body fully blocked the tag, this path is still identified and well tracked;
- 2) The polarplot of the path's trajectory forms a circular shape, indicating the path delay remains unchanged during the spin, which is in line with the actual fact that the human's position is not changed.

Next, the numerical results from a measurement of 4.5 meter linear walking under NLoS, in free-space scenario:

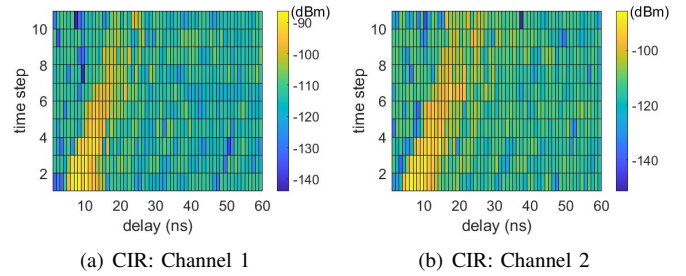


Fig. 22. Channel measurement for a 5 meter NLoS linear walking process

Fig. 22 illustrated the channel measurement for the walking process. As the human is moving away from the anchor, the NLoS attenuation effect on the first path signal becomes stronger. Also we do not observed other obvious cluster of peaks other than the first path, indicating that in this free space scenario no multipath is measured.

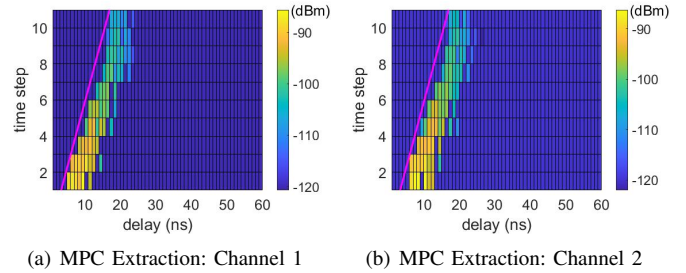


Fig. 23. Multipath extraction from previous channel measurement

Similar to spin process, we performed multipath extraction algorithm on the measurement result which is displayed in Fig. 23. In the result, we specified the ground truth with a pink trajectory, which is in theory the signal arrival delay with

regard to the actual position of the human. To track this path, we implemented multipath tracking algorithm, and the results are shown in Fig. 24

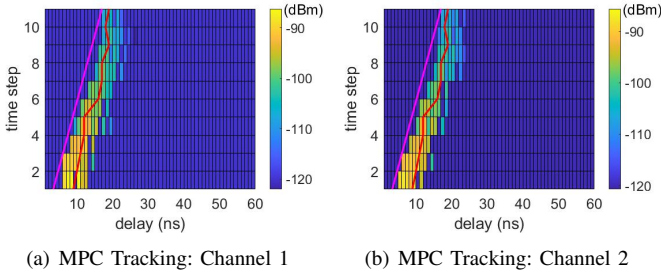


Fig. 24. Multipath tracking over temporal samples, with red line for tracking trajectory and pink line for ground truth. The discrepancy between the tracking trajectory and the ground truth is 4.5 ns on average, yielding to a path difference of 1.35m

The tracking trajectory follows the signal cluster well. Compared to the ground truth, the tracking trajectory is in accordance with the actual moving pattern, despite a delay shift from the theoretical signal arrival. This is because the tracking algorithm always track the strongest peak among all the extracted signal, and such trajectory is always few delay bins after the first arrival of this signal. This observation is the key reason why using VA alone is not sufficient to estimate the tag’s position, and it also yields inspiration on only associating the change of multipath with the change of human’s position. Results prove that this scheme works, which will be shown later in the validation of NLoS localization.

Intuitively, there is no other paths observed in free-space scenario. Next, we move to one-wall scenario, where a huge metal wall is located at 6.7 meters away from the anchor. To simplify the paper, we only present the results from one channel, as are given in Fig. 25.

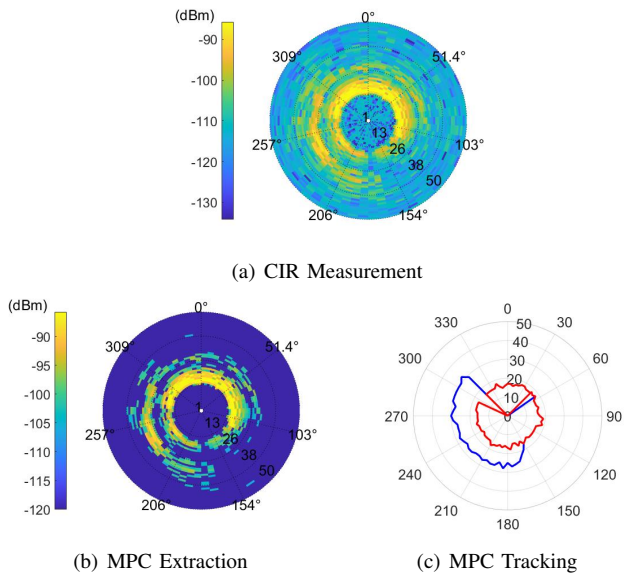


Fig. 25. Body Spin in One-Wall Scenario

As we can see from the results, multipaths are well extracted and tracked during this spin process. At certain orientation range, in this case between approximately 180 and 300 degrees, a clustering of peaks emerges in Fig. 25(a). Associating with the measurement scenario, we believe this is the multipath from the metal wall. After multipaths extraction and tracking, we detect two path trajectories, which are the direct path and the multipath from the wall. Similar to the observation in free space, the path trajectories remains within a small range of delay bins, indicating the position of human is static during the spin. Also, another valuable observation is that during the whole spin, we can always track one or more multipaths. This means if the body stops spin at certain orientation and start walking, there would be at least one path we could make use of for NLoS localization.

Then, we measured a NLoS linear walking, starting from two meters from the anchor, moving along a straight line vertical to the wall for 5 meters and then stopped. Channel measurement, multipaths extraction and tracking are demonstrated in Fig. 26:

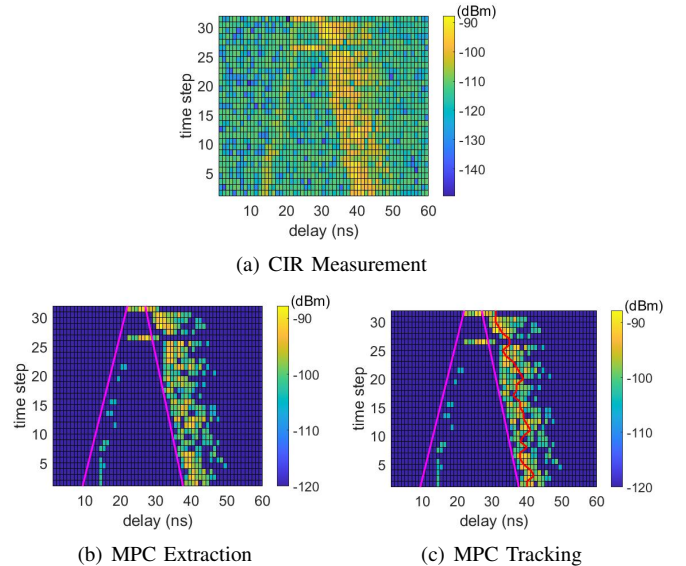


Fig. 26. NLoS linear walking in One-Wall Scenario

The pink line in Fig. 26(b)26(c) are the ground truths for direct path (left) and multipath from the wall (right). From the results, we can see that the first path is significantly attenuated, showing only extracted peaks along the ground truth. However, a strong multipath signal reflected from the wall is detected, so that we could track this multipath during the whole walking process. Compared with the ground truth, this multipath trajectory follows in line with the change of human body, suggesting that this could be used to predict the tag’s position in NLoS.

As the number of scatterers increase, we could expect more multipaths from the results. Therefore, we did measurement for two motion patterns in a two-wall scenario where two walls are located at 3 and 7 meters away from the anchor. First the spin analysis (Fig. 27):

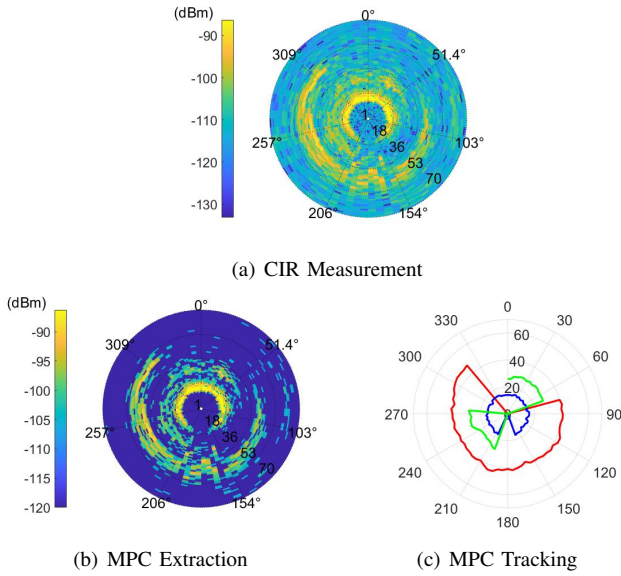


Fig. 27. Body Spin in two-Wall Scenario

Similar to one-wall scenario, we can intuitively identify different signal clusters from the raw CIR measurement in Fig. 27(a). As the major peaks are extracted from the total impulse responses, three paths become clear: the one with the smallest radius, indicating the fastest arrival path, is the first peak, the one with largest radius, and the one vaguely exist in between, are the two multipaths from the wall. The tracking trajectory of the three paths are shown in Fig. 27. As the number of scatterers increase, for all orientation of the human there will be more multipath trajectories that can be used for positioning.

### B. Validation on the Localization Results

After the channel measurement and analysis, we conclude that the extracted multipaths and their tracking trajectory can possible be used for the proposed localization algorithm. In this section, we present the implementation and validation of the whole algorithm. First, a simple validation scenario is designed and shown in Fig. 28.

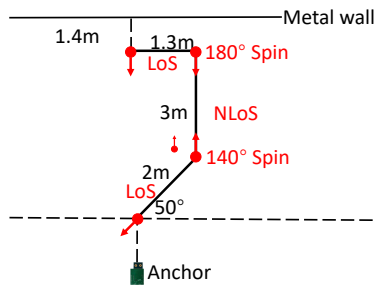


Fig. 28. A simple validation scenario where there is one wall as major scatterer, and the human wearing the tag starts walking with specified orientation along the trajectory. With totally two body spins, the whole walking process are divided as "LoS - NLoS - LoS"

The human starts at the lowest red dot, with  $\beta(t = 0) = 230^\circ$ . The human first walking under LoS till the second red

point, spin counterclockwise for  $140^\circ$  till the body block the tag from anchor. Keep walking down the same orientation to the top right red dot, turn around, and move with LoS to the final destination. Channel and motion measurement are recorded for the whole process, and is later processed on Matlab.

First, the raw localization results from the UWB kit, shown in Fig. 29:

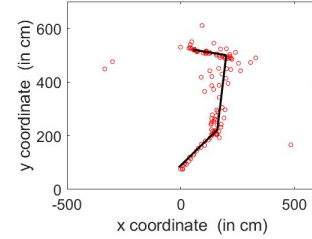


Fig. 29. Localization results from the embedded algorithm of Decawave PDoA kit

Run the scenario identification algorithm based on the channel measurement:

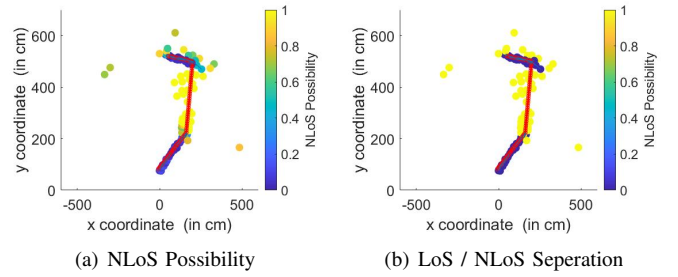


Fig. 30. LoS / NLoS Identification, with red line the ground truth, dots the localization measurement results. In the first figure, the color of the measured points indicates the possibility of NLoS at the time of measurement. Second figure separates the results to LoS (blue) and NLoS (yellow) respectively

The localization results that are identified as NLoS will be discarded, and the position during the NLoS walking is estimated. Next, the motion measurement and spin detection results are shown in Fig. 31. In this case, two spin motions are detected, and from the orientation measurement we derived the spin degree of the two spins  $\Delta\phi(1) = 147.6044^\circ$  and  $\Delta\phi(2) = 169.6628^\circ$  respectively.

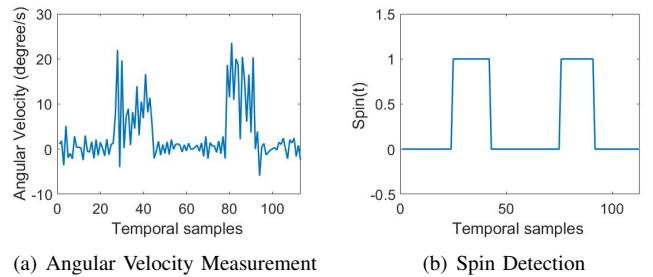


Fig. 31. Spin Detection

On the other hand, we extract and track the multipath from the total CIR, and the results from two channels are displayed in Fig. 32

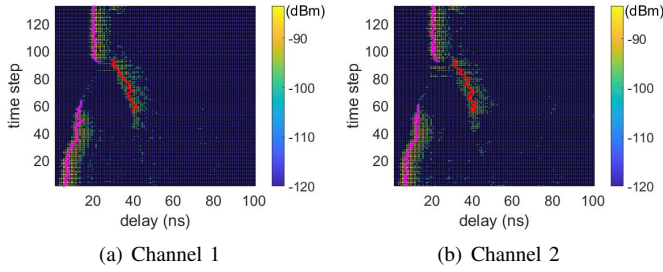


Fig. 32. Spin Detection

During the NLoS walking, the multipath signal is well tracked for the whole process. We take the average of the two tracking trajectory from different channels, and estimate the positions during NLoS together with the orientation information. Finally, the localization result with NLoS estimation is illustrate in Fig. 33.

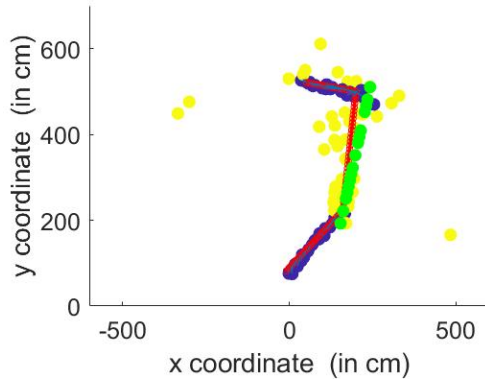


Fig. 33. Localization results with NLoS estimation, shown in green dots. The yellow dots are the NLoS measurement and will be discarded, and the green estimation results will be kept, as final output

Compared with the measurement results (yellow dots), the estimated results (green dots) is visually more close to ground truth. To show how much improvement on accuracy does the algorithm achieves, we define the localization error, as the distance between ground truth and localization results:

$$Error(t) = |P_{GroundTruth} - P| \quad (23)$$

Calculate the localization error, and the results are shown in Fig. 34

Numerically, the average error for measurement and localization results are 48.3328cm and 31.6776cm, and the root mean square error are 88.7612cm and 39.1328cm respectively. Based on the results, we can conclude that the localization algorithm with NLoS estimation provide significant improvement compared to raw measurement.

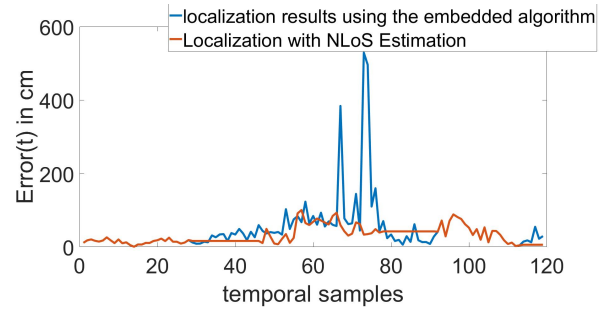


Fig. 34. Localization Error

## VI. CONCLUSION

In this paper, a human localization strategy is presented, with special focus on NLoS caused by self-body blockage, and corresponding solutions where multipaths and motion measurements are involved. From the measurement analysis, we found that the extracted and tracked multipaths showed corresponding characteristics under linear and spin motions, which are further used for localization. At the same time, the inertial measurement provided us with helpful information about the heading of the human object. Together with the dynamic change of multipaths, NLoS human localization is achieved.

The algorithm works well under the assumption of this research. However, the motion pattern for a human may become more complex in reality, e.g. the human is running while the orientation is gradually shifted. Also, the potential of IMU in this research was not fully investigate, since the linear acceleration is abandoned due to accumulated deviation after integration. However, it is definitely worthy to study how to fuse the whole motion measurement data with multipaths information. Additionally, the experiment environment in this research guaranteed certain strong multipaths signals, which may not always be the case in real world applications, e.g. an indoor scenario, where scatterers are made of different materials and distributed randomly in the environment. At that time, association between the tracked multipaths and the scatterers in the environment will be needed for future localization use. The proposed algorithm is also not ready for real time application due to the heavy computational cost to process the channel measurement, as well as the low robustness of the multipath tracking algorithm.

## REFERENCES

- [1] A. Waqar, I. Ahmad, D. Habibi, N. Hart, and Q. V. Phung, "Enhancing athlete tracking using data fusion in wearable technologies," *IEEE Transactions on Instrumentation and Measurement*, vol. 70, pp. 1–13, 2021.
- [2] F. Marins, R. Rodrigues, F. Portela, M. Santos, A. Abelha, and J. Machado, "Extending a patient monitoring system with identification and localisation," in *2013 IEEE International Conference on Industrial Engineering and Engineering Management*, 2013, pp. 1082–1086.
- [3] A. Alarifi, A. Al-Salman, M. Alsaleh, A. Alnafessah, S. Al-Hadhrani, M. A. Al-Ammar, and H. S. Al-Khalifa, "Ultra wideband indoor positioning technologies: Analysis and recent advances," *Sensors*, vol. 16, no. 5, 2016. [Online]. Available: <https://www.mdpi.com/1424-8220/16/5/707>

- [4] I. Dotlic, A. Connell, H. Ma, J. Clancy, and M. McLaughlin, "Angle of arrival estimation using decawave dw1000 integrated circuits," in *2017 14th Workshop on Positioning, Navigation and Communications (WPNC)*, 2017, pp. 1–6.
- [5] H. Liu, H. Darabi, P. Banerjee, and J. Liu, "Survey of wireless indoor positioning techniques and systems," *IEEE Transactions on Systems, Man, and Cybernetics, Part C (Applications and Reviews)*, vol. 37, no. 6, pp. 1067–1080, 2007.
- [6] Decawave, "Application note dw1000 metrics for estimation of non line of sight operating conditions," vol. 10, p. 2018, 3.
- [7] A. A. Wardhana, E. Clearesta, A. Widyotriatmo, and Suprijanto, "Mobile robot localization using modified particle filter," in *2013 3rd International Conference on Instrumentation Control and Automation (ICA)*, 2013, pp. 161–164.
- [8] S. Marano, W. M. Gifford, H. Wymeersch, and M. Z. Win, "Nlos identification and mitigation for localization based on uwb experimental data," *IEEE Journal on selected areas in communications*, vol. 28, no. 7, pp. 1026–1035, 2010.
- [9] H. Wymeersch, S. Marano, W. M. Gifford, and M. Z. Win, "A machine learning approach to ranging error mitigation for uwb localization," *IEEE transactions on communications*, vol. 60, no. 6, pp. 1719–1728, 2012.
- [10] P. Meissner, E. Leitinger, M. Fröhle, and K. Witrisal, "Accurate and robust indoor localization systems using ultra-wideband signals," *arXiv preprint arXiv:1304.7928*, 2013.
- [11] J. Kulmer, S. Hinteregger, B. Großwindhager, M. Rath, M. S. Bakr, E. Leitinger, and K. Witrisal, "Using decawave uwb transceivers for high-accuracy multipath-assisted indoor positioning," in *2017 IEEE International Conference on Communications Workshops (ICC Workshops)*, 2017, pp. 1239–1245.
- [12] K. Witrisal and P. Meissner, "Performance bounds for multipath-assisted indoor navigation and tracking (mint)," in *2012 IEEE International Conference on Communications (ICC)*, 2012, pp. 4321–4325.
- [13] C. Gentner, T. Jost, W. Wang, S. Zhang, A. Dammann, and U.-C. Fiebig, "Multipath assisted positioning with simultaneous localization and mapping," *IEEE Transactions on Wireless Communications*, vol. 15, no. 9, pp. 6104–6117, 2016.
- [14] E. Leitinger, F. Meyer, F. Hlawatsch, K. Witrisal, F. Tufvesson, and M. Z. Win, "A belief propagation algorithm for multipath-based slam," *IEEE Transactions on Wireless Communications*, vol. 18, no. 12, pp. 5613–5629, 2019.
- [15] H. Zhang, Z. Zhang, R. Zhao, J. Lu, Y. Wang, and P. Jia, "Review on uwb-based and multi-sensor fusion positioning algorithms in indoor environment," in *2021 IEEE 5th Advanced Information Technology, Electronic and Automation Control Conference (IAEAC)*, vol. 5, 2021, pp. 1594–1598.
- [16] M. Kok, J. D. Hol, and T. B. Schön, "Indoor positioning using ultra-wideband and inertial measurements," *IEEE Transactions on Vehicular Technology*, vol. 64, no. 4, pp. 1293–1303, 2015.
- [17] Y. Zhang, N. Wang, M. Li, X. Sun, and Z. Wang, "Indoor relative positioning method and experiment based on inertial measurement information/human motion model/uwb combined system," in *2020 27th Saint Petersburg International Conference on Integrated Navigation Systems (ICINS)*, 2020, pp. 1–6.
- [18] H. Benzerrouk and A. V. Nebylov, "Robust imu/uwb integration for indoor pedestrian navigation," in *2018 25th Saint Petersburg International Conference on Integrated Navigation Systems (ICINS)*, 2018, pp. 1–5.
- [19] I. Kashiwagi, T. Taga, and T. Imai, "Time-varying path-shadowing model for indoor populated environments," *IEEE Transactions on Vehicular Technology*, vol. 59, no. 1, pp. 16–28, 2010.
- [20] K. Kitao, N. Tran, T. Imai, and Y. Okumura, "Frequency characteristics of changes in received levels by human body blockage in indoor environment," in *2016 URSI Asia-Pacific Radio Science Conference (URSI AP-RASC)*, 2016, pp. 373–376.
- [21] Decawave, "Dw1000 user manual," 2017.
- [22] —, "Beta pdoa kit user manual," 2018.
- [23] Xsens, "Xsens dot user manual," 2020.
- [24] J. Högbom, "Aperture synthesis with a non-regular distribution of interferometer baselines," *Astronomy and Astrophysics Supplement Series*, vol. 15, p. 417, 1974.
- [25] V. Kristem, S. Sangodoyin, C. U. Bas, M. Käske, J. Lee, C. Schneider, G. Sommerkorn, C. J. Zhang, R. S. Thomä, and A. F. Molisch, "3d mimo outdoor-to-indoor propagation channel measurement," *IEEE Transactions on Wireless Communications*, vol. 16, no. 7, pp. 4600–4613, 2017.
- [26] R.-M. Cramer, R. Scholtz, and M. Win, "Evaluation of an ultra-wide-band propagation channel," *IEEE Transactions on Antennas and Propagation*, vol. 50, no. 5, pp. 561–570, 2002.
- [27] R. Schmidt, "Multiple emitter location and signal parameter estimation," *IEEE Transactions on Antennas and Propagation*, vol. 34, no. 3, pp. 276–280, 1986.
- [28] B. Fleury, M. Tschudin, R. Heddergott, D. Dahlhaus, and K. Inge-man Pedersen, "Channel parameter estimation in mobile radio environments using the sage algorithm," *IEEE Journal on Selected Areas in Communications*, vol. 17, no. 3, pp. 434–450, 1999.
- [29] A. F. Molisch, *Wireless communications*. John Wiley & Sons, 2012, vol. 34.
- [30] C. Lai, R. Sun, C. Gentile, P. B. Papazian, J. Wang, and J. Senic, "Methodology for multipath-component tracking in millimeter-wave channel modeling," *IEEE Transactions on Antennas and Propagation*, vol. 67, no. 3, pp. 1826–1836, 2019.
- [31] J. Maceraudi, F. Dehmas, B. Denis, and B. Uguen, "Multipath components tracking adapted to integrated ir-uwb receivers for improved indoor navigation," in *2016 24th European Signal Processing Conference (EUSIPCO)*, 2016, pp. 753–757.
- [32] W. Wang, T. Jost, and A. Dammann, "Estimation and modelling of nlos time-variant multipath for localization channel model in mobile radios," in *2010 IEEE Global Telecommunications Conference GLOBECOM 2010*, 2010, pp. 1–6.
- [33] M. Froehle, P. Meissner, and K. Witrisal, "Tracking of uwb multipath components using probability hypothesis density filters," in *2012 IEEE International Conference on Ultra-Wideband*, 2012, pp. 306–310.
- [34] K. Mahler, W. Keusgen, F. Tufvesson, T. Zemen, and G. Caire, "Tracking of wideband multipath components in a vehicular communication scenario," *IEEE Transactions on Vehicular Technology*, vol. 66, no. 1, pp. 15–25, 2017.
- [35] D. E. Clark and J. Bell, "Multi-target state estimation and track continuity for the particle phd filter," *IEEE Transactions on Aerospace and Electronic Systems*, vol. 43, no. 4, pp. 1441–1453, 2007.